Journal of Applied Informatics and Computing (JAIC)
Vol.10, No.4, August 2026, pp. 3535~3542
e-ISSN: 2548-6861

Brain Tumor Classification in MRI Images Using Convolutional Neural Networks with Explainable Artificial Intelligence

Muhammad Abdul Ghofur [1*], Nirma Ceisa Santi [2*], Hastie Audytra [3*]
[*] Department of Information Systems, Faculty of Science and Technology, Universitas Nahdlatul Ulama Sunan Giri
ghofur@unugiri.ac.id [1], nirmaceisa@unugiri.ac.id [2], hastie@unugiri.ac.id [3]

Article Info

Article history:

Received 2026-07-07
Revised 2026-07-27
Accepted 2026-08-10

Keyword:

EfficientNetB0,
ResNet50,
Transfer Learning,
5-Fold Cross-Validation.

ABSTRACT

Brain tumors are a condition requiring rapid and accurate diagnosis. This study aims to enhance the transparency of Convolutional Neural Network (CNN)-based brain tumor classification models by implementing Explainable Artificial Intelligence (XAI) techniques, specifically Eigen-CAM and LIME. The models were developed using a transfer learning approach on ResNet50 and EfficientNetB0 architectures, utilizing a dataset of 3,000 MRI images categorized into glioma, meningioma, and pituitary tumor classes. Test results indicate that ResNet50 achieved the best performance, with accuracy, precision, recall, and F1-score values of 94%, while EfficientNetB0 achieved 93%. The application of 5-fold cross-validation improved the models' generalization capabilities and reduced the risk of overfitting. Visualizations using Eigen-CAM and LIME demonstrate that the models focus on relevant tumor regions, thereby increasing the transparency and reliability of MRI-based classification.

I. INTRODUCTION

The brain is a vital organ that controls the body's physiological activities and serves as an information processing center. Brain tissue is composed of neurons and glial cells; uncontrolled cell growth within this tissue can lead to brain tumors [1]. Brain tumors are classified into two main types: primary tumors, which originate from the brain tissue itself, and secondary (metastatic) tumors, which spread from other organs [2]. Common types of primary brain tumors include gliomas, meningiomas, and pituitary adenomas [3]. Early detection and accurate diagnosis are crucial for improving treatment success rates, given that delayed diagnosis often results in lower recovery rates [4].

In clinical practice, medical imaging modalities such as Magnetic Resonance Imaging (MRI) and Computed Tomography (CT scans) are widely used to detect brain tumors [5]. Although effective at identifying lesions, the processes of medical image segmentation and analysis remain complex, require radiologist expertise, and are relatively time-consuming [6]. This situation has driven the development of artificial intelligence-based diagnostic systems to enhance efficiency and accuracy.

One approach demonstrating significant performance in medical image analysis is Deep Learning, particularly through Convolutional Neural Network (CNN) architectures. CNNs are designed to automatically extract features via convolution operations, making them effective at recognizing complex visual patterns in medical images [7]. he application of CNNs has driven a shift from conventional diagnostic methods toward automated diagnostic systems with high accuracy [8].

One CNN architecture that has demonstrated high performance across various image classification tasks is the Residual Network, or ResNet. ResNet addresses the vanishing gradient problem in deep network training through the use of skip connections—or residual blocks—which allow information to pass through multiple layers without losing clarity [9]. ResNet variants consist of several configurations—including ResNet-18, ResNet-34, ResNet-50, and ResNet-101—each with a different number of layers. ResNet-50 is a popular choice for medical image classification because it offers a balance between network depth and computational efficiency [10]. *ResNet-50 has been applied in various medical classification studies with promising results*. [11] demonstrates that pre-trained models

such as EfficientNet and ResNet achieve high accuracy in skin cancer classification based on dermoscopy images.

Research by [9] titled "Brain Tumor Image Classification Using Transfer Learning Techniques on the ResNet-50 Architecture," classified three types of brain tumors (glioma, meningioma, and pituitary) using a transfer learning-based ResNet-50 CNN. The dataset consisted of 3,064 MRI images processed via 224×224 pixel resizing, normalization, and augmentation, and was split using an 80:20 ratio. The model employed the Adam optimizer and was evaluated using standard classification metrics. The results showed a peak accuracy of 91.86%, demonstrating the effectiveness of ResNet-50 for MRI-based brain tumor classification.

The study conducted in [12] utilized the ResNet50 architecture for MRI-based brain tumor classification using a transfer learning approach. The dataset consisted of brain tumor images divided into training, validation, and test sets, processed at a standard input size of 224×224 pixels. The model was trained using the Adam optimizer and demonstrated excellent performance with high accuracy, indicating that ResNet50 is capable of effectively extracting key features from MRI images to distinguish between brain tumor types.

Research by [13] using EfficientNetB0 for glioblastoma classification on 4,465 MRI images demonstrated an accuracy of 88.51%, which increased to 89.70% following the application of intensity normalization preprocessing. Other preprocessing methods such as CLAHE, denoising, and skull stripping reduced the model's performance. Grad-CAM visualization also confirmed that the model was able to focus its attention on the tumor area more accurately after the optimal preprocessing was applied.

The study conducted by [14], titled "Brain Tumor Classification Based on MRI Images Using the EfficientNetV2-S Convolutional Neural Network Method," utilized the EfficientNetV2-S architecture to classify brain tumor MRI images. The dataset employed consisted of MRI images that had undergone preprocessing and were split into training and testing sets. The results demonstrated that the EfficientNetV2-S model achieved high classification performance with excellent accuracy, making it effective for supporting medical image-based brain tumor diagnosis.

Although CNNs have demonstrated excellent performance in medical image classification, a major challenge in their deployment is the tendency for these models to function as "black boxes." This characteristic makes the decision-making process difficult for medical professionals to understand, potentially undermining trust in the system's use within clinical practice. To address this issue, Explainable Artificial Intelligence (XAI) approaches have been developed to enhance transparency and provide explanations regarding the basis of the model's decisions [15].

The application of XAI enables the visualization of MRI image regions that contribute most significantly to classification results, thereby making the model easier to interpret. In addition to boosting user confidence, the resulting interpretability can also support the clinical validation process for automated diagnostic outcomes.

Based on this, this study aims to develop an MRI-based brain tumor classification system using CNN architectures—specifically ResNet50 and EfficientNetB0—integrated with the XAI methods Eigen-CAM and LIME. This combination of approaches is expected to yield a system that not only achieves high classification accuracy in identifying brain tumor types but also provides visualizations explaining the basis of the model's decision-making. Consequently, the proposed system is expected to support a more accurate, transparent, and trustworthy brain tumor diagnosis process.

II. METHODOLOGY

The research process comprises several key stages: data collection, data preprocessing, deep learning modeling, data splitting, model training, model evaluation, and XAI interpretation. The overall workflow of this research process is illustrated in Figure 1.

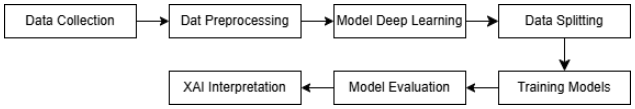

Figure 1 Research Stages

A. Data Collection

This study utilizes a public dataset from Kaggle consisting of 3,000 RGB medical images, each with dimensions of 224 × 224 × 3 pixels. The dataset was curated to ensure class balance and avoid duplication, and was divided into three categories glioma, meningioma, and pituitary with 1,000 images in each. The dataset is based on the Brain Tumor Detection project (https://www.kaggle.com/code/myriamgam62/yolov11-brain-tumor-detection), with the distribution details presented in Table I.

TABLE I
BREAKDOWN OF DATASET SIZES

No.	Class	Quantity
1	*Glioma*	1000
2	*Meningioma*	1000
3	*Pituitary*	1000
	Total	3000

B. Data Preprocessing

Data preprocessing was performed to prepare the images prior to training the CNN model. All images were resized to 224 × 224 pixels and normalized using a preprocessing function compatible with the model architecture. To enhance data diversity and mitigate the risk of overfitting, data augmentation techniques—specifically rotation, shifting, shearing, zooming, and horizontal flipping—were applied.

Subsequently, the model was trained using the Adam optimizer, a batch size of 32, and 20 epochs. This configuration aimed to ensure a stable training process and improve the model's generalization capability.

C. Model Deep Learning

At this stage, the classification process is carried out using a deep learning model based on a Convolutional Neural Network (CNN). The CNN is a deep learning architecture widely used for classifying two-dimensional data, such as images and video. It operates by automatically extracting features through convolution operations, enabling it to effectively recognize patterns and identify objects within images [7]. The specific CNN architecture employed in this study is described below.

1) ResNet50: In 2015, Microsoft Research Asia introduced ResNet (Residual Network) as a solution to the vanishing gradient problem in deep neural networks. This architecture achieved success in the ILSVRC 2015 competition through the ResNet50 variant, which consists of 50 layers. The primary advantage of ResNet lies in the concept of residual learning, which utilizes skip connections; this enables a more stable and efficient training process and allows the network to learn more complex feature representations [16].

2) EfficientNetB0: EfficientNetB0 is a variant of the EfficientNet architecture developed by Google AI with the aim of producing a computationally efficient model without compromising performance. This architecture is based on the concept of compound scaling—proportionally increasing network depth, width, and resolution to optimize performance. EfficientNetB0 serves as the baseline model within the EfficientNet family; despite having a relatively small number of parameters, it delivers high classification performance. Its architectural structure consists of repeating blocks based on depthwise separable convolutions combined with the Swish activation function, thereby enhancing computational efficiency while maintaining the quality of feature extraction [17].

D. Data Splitting

At this stage, partitioning the data into training, validation, and test sets plays a crucial role in determining model performance [18]. In this study, model evaluation for the ResNet50 and EfficientNetB0 architectures was conducted using the K-Fold Cross-Validation technique to obtain a more comprehensive and robust performance assessment. This method enables the optimization of training parameters and mitigates bias associated with a single data split [19]. In general, K-Fold Cross-Validation operates by dividing the dataset into *k* subsets of approximately equal size; the model is then trained and tested over *k* iterations, with each subset serving as the test set in turn while the remaining subsets act as the training data [20]. The steps for K-Fold Cross-Validation are as follows:

- The total dataset is divided into *k* parts.
- In the first fold, the first part serves as the testing data, while the remaining parts serve as the training data. Subsequently, the accuracy defined as the closeness of a measurement result to the actual value or data is calculated based on this data portion. This accuracy calculation utilizes equation (1).

$$Accuracy = \frac{\sum correctly\ classified\ test\ data}{\sum total\ test\ data} \times 100 \quad (1)$$

- The second fold occurs when the second part serves as the testing data and the remainder serves as the training data; then, calculate the accuracy based on that data split.
- Continue this process up to the k-th fold. Calculate the average accuracy from the k accuracy values obtained. This average accuracy becomes the final accuracy.

E. Training Models

During the training phase, hyperparameter tuning was performed to ensure optimal model learning. The model utilized the Adam optimizer with a learning rate of 0.001 and the sparse categorical cross-entropy loss function for multi-class classification. Training was conducted with a batch size of 32 over 20 epochs. Additionally, an ImageNet-based pre-trained model was employed, with fine-tuning applied to the final layers to adapt it to the characteristics of the brain tumor dataset. The model was implemented using the TensorFlow framework with GPU acceleration, resulting in a stable model with good generalization capabilities.

F. Model Evaluation

At this stage, the system is evaluated using a confusion matrix to calculate Accuracy, Precision, Recall, and F-1 score [21]. The equations for calculating Accuracy, Precision, Recall, and F-1 score are presented in equations (2), (3), (4), and (5).

$$Accuracy = \frac{\mathrm{TP} + \mathrm{TN}}{\mathrm{TP} + \mathrm{TN} + \mathrm{FP} + \mathrm{FN}} \quad (2)$$

$$Precision = \frac{\mathrm{TP}}{\mathrm{TP} + \mathrm{FP}} \quad (3)$$

$$Recall = \frac{\mathrm{TP}}{\mathrm{TP} + \mathrm{FN}} \quad (4)$$

$$F - 1\ score = 2\ \mathrm{X}\ \frac{\mathrm{PrecisionXRecall}}{\mathrm{Precision} + \mathrm{Recall}} \quad (5)$$

True Positive (TP): The number of positive data points correctly identified by the system. True Negative (TN): The number of negative data points correctly identified by the system. False Positive (FP): The number of data points that should be negative but are classified as positive by the system. False Negative (FN): The number of data points that should be positive but are classified as negative by the system.

G. XAI Interpretation

The application of Explainable Artificial Intelligence (XAI) in this study focuses on explaining the decision-making process of a CNN model used for skin cancer classification. XAI is a branch of Artificial Intelligence (AI) that aims to enhance transparency by making model predictions and decisions more understandable to humans. Many AI models operate as "black boxes," making their decision-making processes difficult for users to comprehend. XAI addresses this by developing methods that enable users to understand how models generate predictions and decisions [22]. Some common XAI methods used to improve model understanding include:

- *LIME (Local Interpretable Model-agnostic Explanations)*

LIME is a method that provides local explanations for model predictions by constructing a simpler, interpretable model around the prediction generated by a complex model [23]. According to research by [24] the Explainable AI (XAI) technique utilizing LIME (Local Interpretable Model-agnostic Explanations) was selected due to its ability to provide more transparent and easily understandable explanations regarding the recommendations generated by the system. LIME operates by calculating the probability of each feature's contribution to the prediction outcome. Subsequently, the LIME method is integrated into the previously developed model, which employs a user-based Collaborative Filtering approach. The LIME formula is presented in Equation (6).

$$\xi(x) = \underset{g \in \mathrm{G}}{\operatorname{argmin}} \left(L^{lim\,E}\,(f, g, \pi x^{LIME}) + \Omega(g) \right) \quad (6)$$

f is a complex model (such as a CNN). $\mathrm{g} \in \mathrm{G}$ is an interpretable model (such as linear regression or a decision tree). πx is a local distribution around x used for sample weighting. $\Omega(g)$ is a regularization function that controls the complexity of model g, to ensure it remains interpretable. $L^{lim\,E}\,(f, g, \pi x^{LIME})$ is a squared loss function that measures the distance between f and g with G representing the class of model explanations ($g \in \mathrm{G}$). πx^{LIME} represents a measure of proximity around the input data x to be explained.

- *Eigen-CAM*

Eigen-CAM is a newer interpretability method used to visualize the most relevant features in model predictions, particularly in the context of images. Unlike Grad-CAM, which operates based on gradients, Eigen-CAM identifies important areas within an image by analyzing the eigenvalues of layer activations in Convolutional Neural Networks (CNNs); this enables more accurate and reliable explanations for medical applications, such as skin cancer detection [25]. Eigen-CAM advances visualization techniques by utilizing principal components to generate more efficient and detailed activation maps, thereby introducing a novel approach to exploring relevant regions within images [26].

III. Result and Discussion

A. Training Results on the Model

Table 2 shows that ResNet50 yields better classification performance than EfficientNetB0 across all evaluation metrics. ResNet50 achieved accuracy, precision, recall, and F1-score values of 94%, whereas EfficientNetB0 reached 93% for each metric. Although the performance difference is relatively small, these results indicate that ResNet50 is more effective at extracting image features, thereby enabling more accurate and consistent classification.

TABLE 1
RESEARCH RESULTS FOR THE MODEL

Model	Accuracy	Precision	Recall	F1-Score
ResNet50	94%	94%	94%	94%
EfficientNetB0	93%	93%	93%	93%

B. Classification Report Evaluation

Based on the classification reports shown in Figures 2 and 3, the ResNet50 model demonstrated superior classification performance compared to EfficientNetB0. ResNet50 achieved an overall accuracy of 94%, with average precision, recall, and F1-score values of 0.94 each. At the class level, the model attained F1-scores of 0.96 for glioma, 0.91 for meningioma, and 0.95 for pituitary tumors. Meanwhile, EfficientNetB0 yielded an accuracy of 93% with average precision, recall, and F1-scores of 0.93, and class-specific F1-scores of 0.95 for glioma, 0.89 for meningioma, and 0.94 for pituitary tumors. These results indicate that while both models possess good classification capabilities, ResNet50 delivers slightly superior and more consistent performance in distinguishing between the three types of brain tumors in MRI images.

```
====== CLASSIFICATION REPORT ======
              precision    recall  f1-score   support

      glioma       0.98      0.94      0.96      1000
  meningioma       0.91      0.90      0.91      1000
   pituitary       0.92      0.97      0.95      1000

    accuracy                           0.94      3000
   macro avg       0.94      0.94      0.94      3000
weighted avg       0.94      0.94      0.94      3000
```

Figure 2 Classification Report ResNet50

```
====== CLASSIFICATION REPORT ======
              precision    recall  f1-score   support

      glioma       0.98      0.92      0.95      1000
  meningioma       0.92      0.87      0.89      1000
   pituitary       0.89      0.99      0.94      1000

    accuracy                           0.93      3000
   macro avg       0.93      0.93      0.93      3000
weighted avg       0.93      0.93      0.93      3000
```

Figure 3 Classification Report EfficientNetB0

C. Multi-Class ROC Curve Evaluation

Based on the ROC curves, both the ResNet50 and EfficientNetB0 models demonstrated excellent classification performance, achieving high AUC values across all brain tumor classes. ResNet50 yielded AUC values of approximately 0.95–0.96 for the glioma and pituitary classes and around 0.91 for the meningioma class, with a macro-average AUC approaching 0.94, indicating strong and stable discriminative capability. Meanwhile, EfficientNetB0 also exhibited competitive performance with a similar AUC pattern, although it showed slightly less consistency across classes. Overall, both models were effective at distinguishing between tumor classes, though ResNet50 tended to deliver more optimal performance. The multi-class ROC curve evaluation results are presented in Figures 4 and 5.

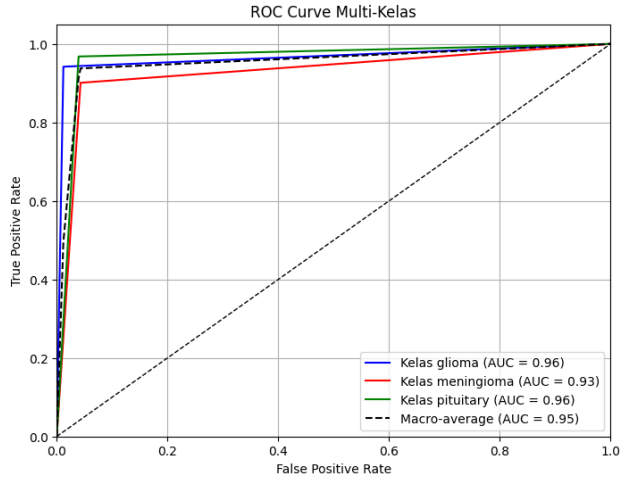

Figure 4 Multi-class ROC Curve for ResNet50

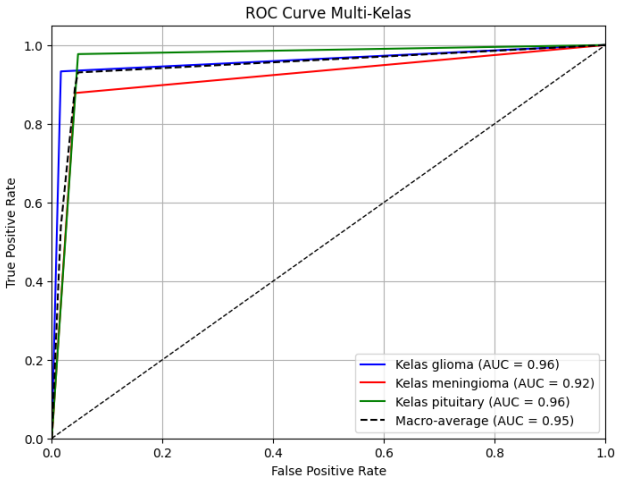

Figure 5 Multi-class ROC Curve for EfficientNetB0

D. Confusion Matrix Evaluation

Based on the confusion matrix, the ResNet50 model (first image) demonstrates excellent classification performance with a high number of correct predictions for each class—942 for glioma, 901 for meningioma, and 968 for pituitary—and a relatively low error rate, although some misclassifications persist, particularly in the meningioma class, which is frequently confused with the pituitary class. Meanwhile, the EfficientNetB0 model (second image) also shows good performance, with correct predictions of 921 (glioma), 868 (meningioma), and 988 (pituitary), respectively; however, it exhibits a slightly higher error rate, especially regarding the meningioma class, which is quite often misclassified as pituitary. Overall, both models are capable of classifying the data effectively, but ResNet50 tends to be more accurate and consistent than EfficientNetB0. The confusion matrix results are presented in Figures 6 and 7.

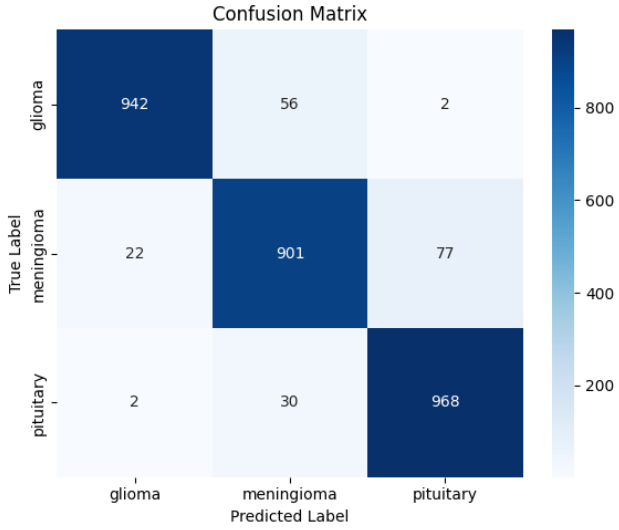

Figure 6 Confusion Matrix ResNet50

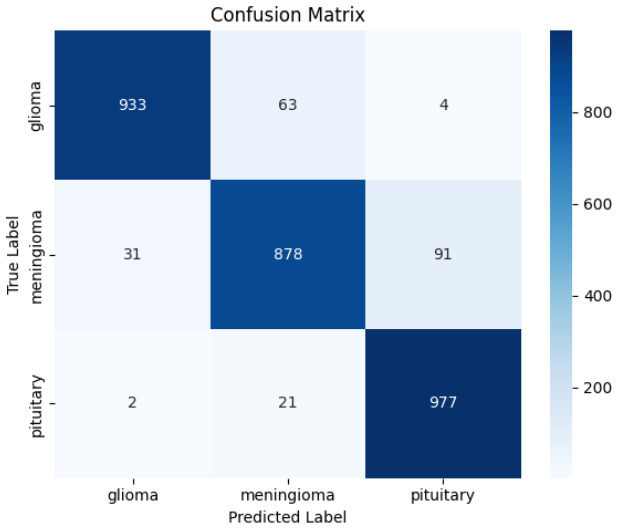

Figure 7 Confusion Matrix EfficientNetB0

E. Accuracy Results for Each Fold Validation

Based on the 5-fold cross-validation results, the ResNet50 model demonstrated relatively stable performance, with accuracy values ranging from 0.9117 to 0.9417, peaking at 0.9417 in Fold 3. Meanwhile, EfficientNetB0 showed an accuracy range of 0.9033 to 0.9383, with its best performance in Fold 2 (0.9383). Overall, ResNet50 tended to yield more consistent and slightly higher results across most folds, whereas EfficientNetB0 also exhibited good generalization capabilities, despite showing slightly greater performance variation between folds. These findings indicate that both models adapt well to data variations; however, ResNet50 holds an advantage in terms of stability and performance consistency, as shown in Table 3.

TABLE 2
VALIDATION ACCURACY RESULTS FOR EACH FOLD

Model	Fold 1	Fold 2	Fold 3	Fold 4	Fold 5
ResNet50	0.9233	0.9250	0.9417	0.9333	0.9117
EfficientNetB0	0.9033	0.9383	0.9117	0.9133	0.9133

F. Comparison with Previous Research

Based on a comparison with previous studies, the methods proposed in this research demonstrate significant performance improvements. Research by [19] using an SVM algorithm achieved an accuracy of 91%, while [20], employing a hybrid CNN and Decision Tree approach, reached 92% accuracy, and [21] achieved 82.14% accuracy using VGG16. In comparison, the models proposed in this study—ResNet50 and EfficientNetB0—achieved accuracies of 94% and 93%, respectively. These results, as shown in Table 4, indicate that utilizing more modern and optimized CNN architectures effectively enhances medical image classification performance.

TABLE 3
COMPARISON WITH REVIOUS STUDIES

Researcher	Model	XAI	Accuracy
[27]	SVM	-	Accuracy 91%
[28]	Hybrid CNN and Decision Tree	-	Accuracy 92%
[29]	VGG16	-	Accuracy 82.14%
[30]	VGG16 and MobileNet	-	Accuracy 92%
Our Proposal	ResNet50	LIME and Eigen-CAM	Accuracy 94%
Our Proposal	EfficientNetB0	LIME and Eigen-CAM	Accuracy 93%

G. XAI model interpretation

Based on the evaluation results, the ResNet50 model demonstrated the best performance among all tested models, achieving Accuracy, Precision, Recall, and F1-score values of 94% each, whereas EfficientNetB0 reached 93%. These results indicate that ResNet50 possesses superior classification capabilities with a lower error rate. To enhance model interpretability, this study employs an Explainable Artificial Intelligence (XAI) approach using LIME and Eigen-CAM techniques. Both methods are utilized to visualize the regions of the brain tumor images that contribute most significantly to the model's decisions, thereby rendering the classification process more transparent and interpretable.

- *Visualization of Eigen-CAM*

Figure 8 shows the Eigen-CAM visualization results, where the ResNet50 model focuses on the tumor area—indicated by red, representing the region with the highest contribution—while colors ranging from yellow to blue represent lower contributions. These results demonstrate that the model is capable of identifying relevant features during the brain tumor classification process.

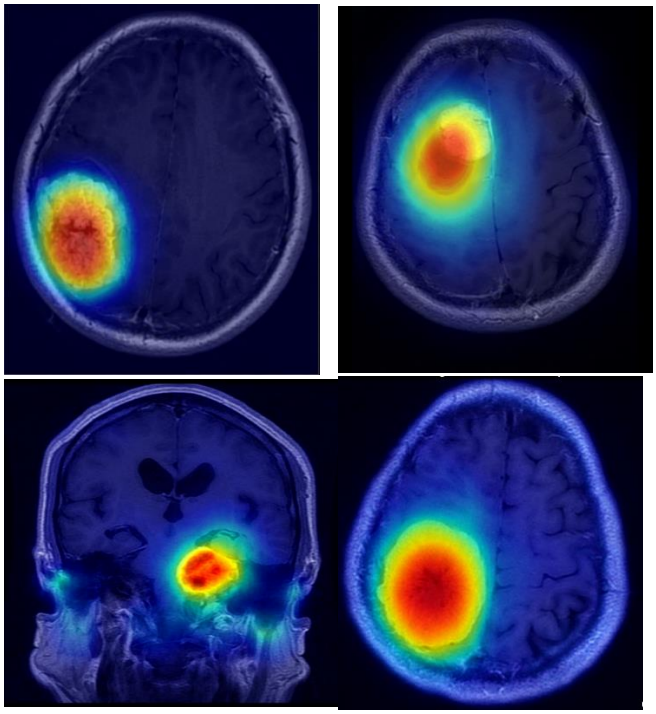

Figure 8 Eigen-CAM Interpretation Results

- *Visualization OF LIME*

Figure 9 shows the visualization results of Local Interpretable Model-agnostic Explanations (LIME) applied to brain tumor MRI images. The green-shaded areas represent the superpixels that contributed most significantly to the model's classification decision. It is evident that the majority of these important superpixels are located within the tumor region, whereas the surrounding brain tissue contributes little

to the prediction. These results demonstrate that the model successfully utilizes relevant features at the tumor site, thereby enhancing the interpretability of and confidence in the classification results.

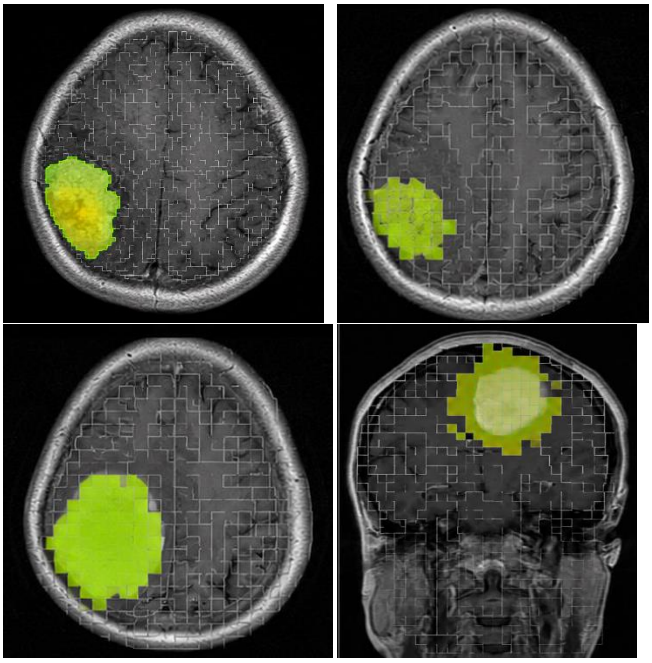

Figure 9 LIME Interpretation Results

H. XAI Interpretation Analysis

To enhance the interpretability of the brain tumor classification model, this study employs Eigen-CAM and LIME. Eigen-CAM results indicate that the model focuses its attention on the tumor area as the primary basis for prediction. Meanwhile, LIME identifies the superpixels that contribute most significantly to the classification, the majority of which are located within the tumor area. These results demonstrate that the model utilizes clinically relevant features, thereby increasing transparency and trust in the classification outcomes.

IV. CONCLUSION

This study aims to enhance the transparency of Convolutional Neural Network (CNN)-based brain tumor classification models by implementing Explainable Artificial Intelligence (XAI) using Eigen-CAM and LIME. Eigen-CAM visualizes the tumor regions that contribute most significantly to the prediction, while LIME identifies the superpixels supporting the model's decision. Test results indicate that ResNet50 achieved the best performance, with accuracy, precision, recall, and F1-score values of 94%, followed by EfficientNetB0, which achieved 93% across all these metrics. Furthermore, the use of 5-fold cross-validation improved the models' generalization capabilities and reduced the risk of overfitting, resulting in an accurate, reliable, and transparent brain tumor classification system.

Based on the research findings, ResNet50 is recommended as the primary model for brain tumor classification due to its superior performance, while EfficientNetB0 serves as a viable alternative for resource-constrained devices. Implementing XAI is advised to enhance the transparency of prediction results, and future research could utilize more diverse datasets while exploring other CNN architectures to improve model accuracy and generalization capabilities.

REFERENCES

[1] Amila, E. Sembiring, A. S. Marbun, A. Prity, H. Agustina, and W. E. M. Purba, "Edukasi Deteksi Dini Dan Pencegahan Tumor Otak Pada Anak Dan Remaja," *Abdimas Mutiara*, vol. 6, no. 1, pp. 169–175, 2025.

[2] U. Sandhya, "Brain tumor detection and classification with DGMM – RBCNN technique," vol. 6, no. April, pp. 7345–7361, 2022.

[3] M. S. Mithun and S. J. Jawhar, "Journal of Radiation Research and Applied Sciences Detection and classification on MRI images of brain tumor using YOLO NAS deep learning model," *J. Radiat. Res. Appl. Sci.*, vol. 17, no. 4, p. 101113, 2024, doi: 10.1016/j.jrras.2024.101113.

[4] V. Le, T. Pham, and C. Author, "Ovarian Tumors Detection and Classification on Ultrasound Images Using One-stage Convolutional Neural Networks," vol. 5, no. 2, pp. 561–581, 2024, doi: 10.18196/jrc.v5i2.20589.

[5] M. Aamir *et al.*, "Brain Tumor Detection and Classification Using an Optimized Convolutional Neural Network," 2024.

[6] B. S. Shukur and M. M. Mijwil, "Involving machine learning techniques in heart disease diagnosis : a performance analysis," vol. 13, no. 2, pp. 2177–2185, 2023, doi: 10.11591/ijece.v13i2.pp2177-2185.

[7] D. P. Mawardi, M. Novita, N. D. Saputro, F. Teknik, and U. Pgri, "Deteksi Awal Klasifikasi Jenis Penyakit Kanker Kulit Dengan Algoritma Convolutional Neural Network (CNN) Berbasis Mobile Apps," vol. 3, no. 2, pp. 1–6, 2024.

[8] I. G. L. Yudha, N. A. Sanjaya ER, A. A. I. N. E. Karyawati, I. B. G. Dwidasmara, I. G. N. A. C. Putra, and I. B. M. Mahendra, "Article Classification Using Convolutional Neural Network (CNN) And Chi-Square Feature Selection," *JELIKU (Jurnal Elektron. Ilmu Komput. Udayana)*, vol. 11, no. 3, p. 529, 2022, doi: 10.24843/jlk.2023.v11.i03.p08.

[9] Y. I. Salsabila, H. Mustofa, and M. A. Ulinuha, "Teknik Transfer Learning Pada Arsitektur Resnet-50," vol. 9, no. 1, pp. 128–139, 2025, doi: 10.52362/jisicom.v9i1.1925.

[10] A. Resnet-, "Klasifikasi Jenis Burung Menggunakan Metode CNN Dan Arsitektur ResNet-50 1,2," vol. 10, no. 3, pp. 34–46, 2023.

[11] K. Ali, Z. Ahmed, A. Ayub, and A. Ali, "Neuroscience Informatics Multiclass skin cancer classification using EfficientNets – a first step towards preventing skin cancer," *Neurosci. Informatics*, vol. 2, no. 4, p. 100034, 2022, doi: 10.1016/j.neuri.2021.100034.

[12] M. B. Kurniawan and E. Utami, "Perbandingan Kinerja ResNet50, VGG16, dan MobileNetV2 untuk Klasifikasi Tumor Otak pada Citra MRI Performance Comparison of ResNet50, VGG16, and MobileNetV2 for Brain Tumor Classification on MRI Images," *Sist. J. Sist. Inf.*, vol. 14, pp. 767–777, 2025.

[13] N. Firdaus *et al.*, "Pengaruh Preprocessing Pada Deteksi Glioblastoma Pada Citra Magnetic Resonance Imaging Dengan," vol. 9, no. 12, pp. 1–11, 2025.

[14] Y. B. Nainggolan, R. S. Perdana, and A. A. Soebroto, "Klasifikasi Penyakit Tumor Otak berdasarkan Citra MRI Menggunakan Metode Convolutional Neural Network EfficientNetV2-S," vol. 9, no. 10, 2025.

[15] J. Teknik, I. Cit, D. Kurniawan, and L. Pujiastuti, "Jurnal Teknik Informatika CIT Medicom yang dapat dipercaya Machine Translated by Google," vol. 15, no. 5, pp. 240–246, 2023.

[16] Q. A. Fitroh and S. Uyun, "Pembelajaran Transfer Mendalam untuk Meningkatkan Klasifikasi Akurasi Gambar Dermoskopi Kanker Kulit," vol. 12, pp. 78–84, 2023.

[17] A. N. Fajrina, Z. H. Pradana, S. I. Purnama, and S. Romadhona, "Penerapan Arsitektur EfficientNet-B0 Pada Klasifikasi Leukimia Tipe Acute Lymphoblastik Leukimia," *J. Ris. Rekayasa Elektro*, vol. 6, no. 1, p. 59, 2024, doi: 10.30595/jrre.v6i1.22090.

[18] H. A. Wahyudi, D., Soesanti, I., & Nugroho, "Optimizing Hyperparameters of YOLO to Improve Performance of Brain Tumor Detection in MRI Images," *2023 6th Int. Conf. Inf. Commun. Technol. (ICOIACT)*, pp. 413–418, 2023, [Online]. Available: https://doi.org/10.1109/ICOIACT59844.2023.10455813

[19] W. Wijiyanto, A. I. Pradana, S. Sopingi, and V. Atina, "Teknik K-Fold Cross Validation untuk Mengevaluasi Kinerja Mahasiswa," *J. Algoritm.*, vol. 21, no. 1, pp. 239–248, 2024, doi: 10.33364/algoritma/v.21-1.1618.

[20] L. Mardiana, D. Kusnandar, and N. Satyahadewi, "Analisis Diskriminan Dengan K Fold Cross Validation Untuk Klasifikasi Kualitas Air Di Kota Pontianak," *Bul. Ilm. Mat. Stat. dan Ter.*, vol. 11, no. 1, pp. 97–102, 2022, [Online]. Available: https://jurnal.untan.ac.id/index.php/jbmstr/article/view/51608

[21] U. Multi, D. Palembang, J. Rajawali, and N. Palembang, "Klasifikasi Kanker Kulit Pada Citra Dermatoskopi Menggunakan CNN 1,2," vol. 5, no. 1, 2024, doi: 10.35957/algoritme.xxxx.

[22] L. Gilpin, L. H., Bau, D., Yuan, B. Z., Bajwa, A., Specter, M., & Kagal, "Explaining explanations: An overview of interpretability of machine learning," *Proc. - 2018 IEEE 5th Int. Conf. Data Sci. Adv. Anal. DSAA 2018*, pp. 80–89, 2018, [Online]. Available: https://doi.org/10.1109/DSAA.2018.00018

[23] M. T. Ribeiro, S. Singh, and C. Guestrin, "'Why Should I Trust You?' Explaining the Predictions of Any Classifier," *NAACL-HLT 2016 - 2016 Conf. North Am. Chapter Assoc. Comput. Linguist. Hum. Lang. Technol. Proc. Demonstr. Sess.*, vol. 2016, no. 1, pp. 97–101, 2016, doi: 10.18653/v1/n16-3020.

[24] M. P. Hendaria, S. Maliawan, U. Pusat, S. Denpasar, and K. S. Skuamosa, "Kanker kulit," pp. 1–17.

[25] F. A. Aschieri, F., Ciabattoni, A., & Genco, "Classical proofs as parallel programs. Electronic Proceedings in Theoretical Computer Science," *EPTCS*, vol. 277, pp. 43–57, 2018, [Online]. Available: https://doi.org/10.4204/EPTCS.277.4

[26] A. Chattopadhay, A. Sarkar, P. Howlader, and V. N. Balasubramanian, "Grad-CAM++: Generalized gradient-based visual explanations for deep convolutional networks," *Proc. - 2018 IEEE Winter Conf. Appl. Comput. Vision, WACV 2018*, vol. 2018-Janua, pp. 839–847, 2018, doi: 10.1109/WACV.2018.00097.

[27] T. A. M and Q. N. Azizah, "Klasifikasi Tumor Otak Menggunakan Ekstraksi Fitur HOG dan Support Vector Machine," *J. Khatulistiwa Inform.*, vol. 4, no. 1, pp. 45–50, 2022, [Online]. Available: https://www.neliti.com/publications/491268/

[28] M. N. M. Hakim, A. B. Nugroho, and A. E. Minarno, "Prediksi Tumor Otak Menggunakan Metode Convolutional Neural Network," *Inform. Mulawarman J. Ilm. Ilmu Komput.*, vol. 17, no. 1, p. 48, 2023, doi: 10.30872/jim.v17i1.5246.

[29] A. B. Wicaksono and B. P. Hartato, "Analisis Performa Arsitektur Cnn Inceptionv3 Dan Vgg16 Dalam Klasifikasi Deteksi Kanker Otak," *JIPI (Jurnal Ilm. Penelit. dan Pembelajaran Inform.*, vol. 10, no. 2, pp. 938–948, 2025, doi: 10.29100/jipi.v10i2.6090.

[30] R. R. Siregar and A. M. Husein, "Klasifikasi Tumor Otak Pada Gambar Magnetic Resonance Images (MRI) Dengan Pendekatan Pembelajaran Mendalam," vol. 4, no. 1, pp. 62–68, 2024.